Supplementary information for

Signal Propagation in Reversible Digital Mechanics

Hilary A. Johnson,*[a+] Robert M. Panas, *[a] Amin Farzaneh, [b] Frederick Sun, [a] Logan Bekker, [a] John Cortes, [a] Melika Ahmadi, [b] Julie Mancini, [a] Andrew J. Pascall, [a] and Jonathan B. Hopkins [b]

* Co-first authors.
Correspondence: johnson491@llnl.gov

Supplementary Information

AND gate and memory bit designs are parametric and tunable to a range of propagation parameters. While transition waves through bistable chains are well-studied, we develop a general model, which we extend to incorporate chains of bistable elements and logic gates. These models are versatile and applicable to designs beyond those demonstrated in this work. Specifically, we discuss the AND gate and memory bit general models, pre-load configurations, and cross-pivot rolling radius, along with propagation regimes, pulse propagation, and the potential energy map calculations. Additionally, we demonstrate circuit synthesis, alternative circuit designs, and micro and macro-fabrication. All designs are compatible with layer-based fabrication methods. The nomenclature section lists all variables.

Throughout this work, parameters are non-dimensionalized to capture scale-independent behaviors. Capital letters represent non-dimensional (n.d.) values. The variables used are standard: L is length, K is stiffness, X and Y are displacements, F is force, and E is energy. The subscript 'b' indicates bistable memory bit, while subscript 'a' denotes an AND gate. Refer to Nomenclature for details about all parameters.

MEMORY BIT

Layered memory bit design

The memory bit is a mechanical bistable element (Fig.S1) with kinematics and energetics layers (Fig.S1a). The kinematics layer is composed of two physical layers to generate the stacked cross-pivot bearing rolling effect and set the kinematics of the memory bit, as shown in the "Memory Bit General Model" section. A cross-pivot architecture, as opposed to conventional blade flexures, were chosen due to superior range per size while retaining the capability to handle high compressive loads, required for bistability. Conventional blade flexures tend to buckle under the combined range and compressive load requirements, resulting in unreliable behavior[1,2]. See section 'Cross-pivot rolling radius' for details.

The Y-axis compliance (axial stiffness, Fig.S1a,b) was placed in series with the motion stage, (located at the center of the memory bit, where gate displacement is measured to indicate the digital state of the bit), using the 4-bars topology to decouple design requirements and simplify the design rather than within the motion stage itself, as has been done with other designs. The symmetric distribution of the Y-axis compliance on both sides of the motion stage suppresses shuttle parasitic Y-axis displacement during operation. Furthermore, the 6 degree of freedom (DOF) coupling linkages decouples memory bit orientations from one another by passing only force without constraining motion (Fig.S1c). The coupling linkage is made as a separate part to facilitate easy assembly for reconfigurable systems.

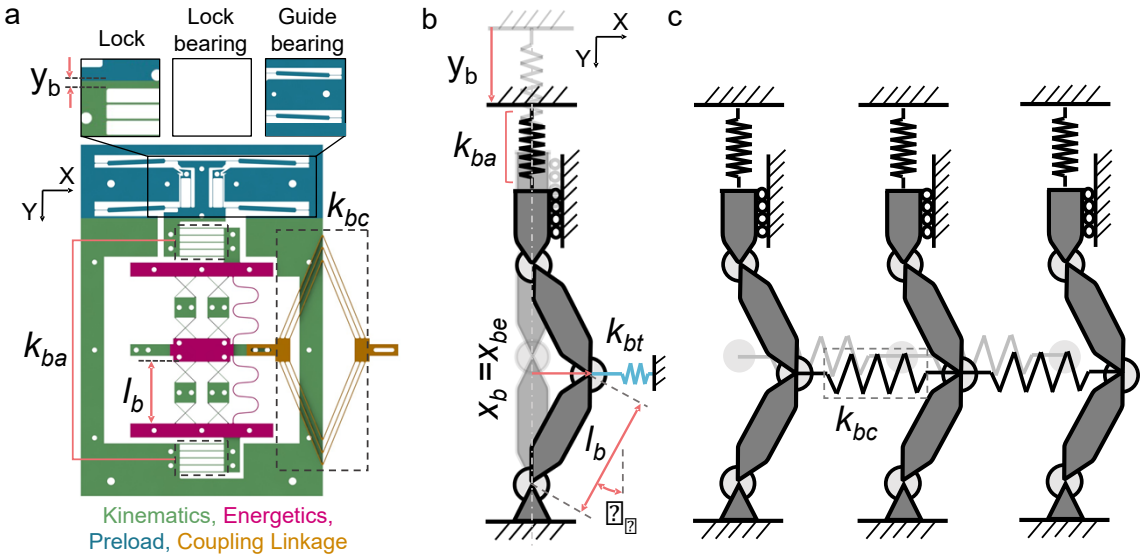

Fig.S1 | Memory bit layers and functional components. a, A memory bit is made up of four layers: kinematics, energetics, preload, and coupling linkage. The axial stiffness bearing and preload mechanism are included in the kinematics layer. The energetics layer, positioned above the kinematics layer, contains 6-DOF compliance elements that add stiffness without restricting motion. The under-constrained coupling linkage is also part of this layer. The preload lock bearing is specifically designed to enable the energization of the bistable element. b, Detailed schematic of a pseudo-rigid body model of a bistable element in its as-fabricated, stress-free, unlocked condition (shadow schematic). In a subsequent step, the

lock is compressed by the amount yb to energize the memory bit and enable bistable behavior (darker schematic). The energized state illustrates the memory bit equilibrium, with parameters mapped onto the generalized structure. kbt is an equivalent stiffness representing stiffness of a memory bit linkages in the x-direction excluding the axial stiffness, kba. c, A chain of three memory bits connected by coupling linkages shown in unenergized and energized states.

The energetics layer contains non-motion-constraining 6 DOF compliance elements (Fig.S1a) that fine-tune each element's unique compliance values required for wave propagation. The energetics layer is laid above the kinematics layer and is composed of additional flexible elements that stack in parallel with the kinematics bearings, providing additional stiffness without constraint. The under-constrained coupling linkage is included in the energetics layer.

Preload design trade-offs

To enable bistable behavior in the memory bit, axial preload is required to induce structural buckling. Unlike traditional beam buckling, structural buckling is achieved through the bending of cross-pivot flexures arranged in both series and parallel configurations. Compatibility with micro-scale additive manufacturing was a critical consideration in the selection of the preload mechanism.

The preload mechanism is printed in series with the memory bit and can include either a latch or a bistable structure. After fabrication, the preload mechanism is actuated and secured, which engages the bistable behavior of the memory bit. Three preload strategies were considered: a latch, a bistable structure, and substrate strain.

The latch design (Fig. S1a) utilizes a nonlinear ratchet to restrict the return motion of a slider that compresses the memory bit's axial spring. This approach provides high stiffness, is easily tunable to achieve the required displacement, and is compatible with both micro- and macro-scale manufacturing.

Alternatively, a bistable structure (Fig. S2a) can be used to produce the required displacement. While this design is tunable and relatively straightforward, it requires a larger footprint and results in reduced axial stiffness of the preload structure, which can negatively impact the memory bit's performance.

The third strategy, substrate strain (Fig. S2b), compresses the printed structures after fabrication by applying strain to the substrate. This approach is compact and preserves the compliance of the memory bit substructure. However, it requires unidirectional compression, significantly limiting design complexity. Additionally, tuning the strain within the structure is challenging due to substrate compliance.

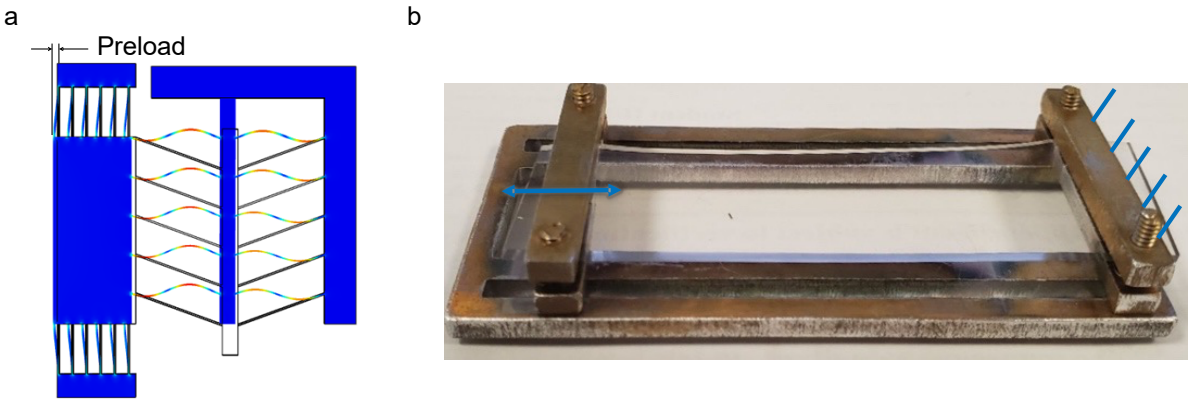

Fig.S2 | A memory bit is charged with stored energy to initiate bi-stability. a, One pre-load strategy is displacing a flexural preload structure. **b,** An alternate pre-load strategy strains the microscale structure substrate, PDMS, pre-print and then relaxes the substrate after manufacturing to charge the elements. The blue arrow shows the substrate strain direction.

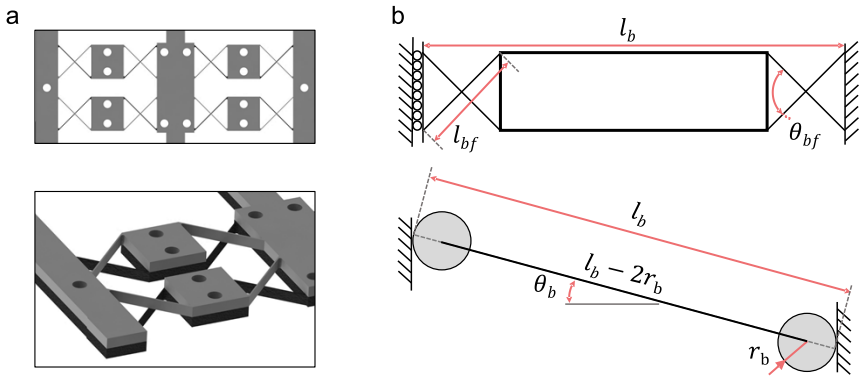

Fig.S3 | Cross-pivot flexures. a, Top and isometric views of the cross-pivot bearing layers. The cross pivots are combined in series and parallel to ensure linear motion of the center shuttle. **b,** Defining geometric parameters of the bearing kinematics.

Cross-pivot rolling radius

Cross-pivots, as shown in Fig.S3, allow motion about a single axis, to first order analysis. A simple model of this behavior is a pin joint. However, the location of the instant center is not actually fixed since the flexures distort and shifts the instant center under large displacements. Thus, the instant center 'rolls' with a horizontal translation that is dependent on the scale of the bearing.

The scale of the pin joint rolling effect is captured by an effective radius r_b, where $r_b = 0$ indicates bearing rotation produces no translation. Any memory bit bearing that can be reduced to a model of rigid bodies linked via pin joints can be modified with rolling behavior. The function defining the rolling radius for cross-pivot bearings was determined by Van Eijk[1], and is included in Eq.(S1), where l_{bf} is the length of cross-pivot flexures, a is the location of the instant center of rotation normalized to the flexure length (a = ½ describes the typical mid-point crossing) and θ_{bf} is the angle between the cross-pivot flexures (Fig.S3b).

$$r_b = \frac{2l_{bf}}{cos\left(\frac{\theta_{bf}}{2}\right)}\left(-\frac{3}{5}a^2 + \frac{3}{5}a - \frac{1}{15}\right) \tag{S1}$$

The rigid link pinned-pinned model is replaced by a rigid link of length l_b-2r_b with rolling contacts of radius r_b added at both ends, shown in Fig.S3b, and a total separation l_b between the rolling surfaces. The shuttle translation, x, combines the rigid body rotation and the edge surface rolling. Rolling effects alter the elasto-mechanics of the memory bit slightly, modifying the force and energy profiles.

Memory bit general model

The general kinematics and energetics memory bit model is parametrically defined by the lever arm characteristic length l_b, axial stiffness k_{ba}, y-axis displacement y_b, transverse stiffness k_{bt}, x-axis displacement x_b, and coupling stiffness k_{bc} (Fig.S1). Degeneracy is required in the bistable states to ensure an equivalent response during signal propagation between states, whether transitioning from 0 to 1 or 1 to 0. Geometric symmetry is the simplest approach to ensure degeneracy. Symmetry requires that the unstressed structure hold the unstable equilibrium position and be energized via the preload, y_b, after fabrication.

These conditions hold regardless of the means of compliance, structure scale, or bistable displacement orientation relative to the chain orientation since the coupling stiffness simply represents the compliance between relative node locations independent of the actual axis these motions. Thus, the general model is useful for analyzing many designs beyond this work when equivalents for l_b, k_{ba}, y_b, k_{bt}, and k_{bc} are identified.

The potential energy of the memory bit, E_b, is stored within the bistable element structure and arises from the compression of the equivalent axial and transverse springs. This energy is a function of the displacements X_b, Y_b, R_b, Eq.(S2).

$$E_b = K_{bt}X_b^2 + \left[Y_b - (2 - 4R_b)(1 - \sqrt{1 - X_b^2})\right]^2 \tag{S2}$$

The energy derivative is the force generated by the memory bit bearing on the node, Eq.(S3).

$$F_{bx} = \left[4(1-2R_b)^2\left(1-\frac{1-\frac{Y_b}{2-4R_b}}{\sqrt{1-X_b^2}}\right)-K_{bt}\right]X_b \tag{S3}$$

The force derivative is the memory bit bearing stiffness on the node, reduced to Eq.(S4).

$$K_{bx} = \left[4(1-2R_b)^2\left(1-\frac{1-\frac{Y_b}{2-4R_b}}{1-X_b^{23/2}}\right)-K_{bt}\right] \tag{S4}$$

A range of important parameters are defined from these expressions, including Eq.(S5) the n.d. scale of the potential energy change from bistable equilibrium to unstable equilibrium (Fig.2a,b), ΔE_{bMax}, Eq.(S6) the n.d. minimum potential energy at bistable equilibrium, E_{bMin}, Eq.(S7) the n.d. relative memory bit potential energy, ΔE_b, Eq.(S8) the n.d. memory bit potential energy profile, ΔE_{bp} plotted in Fig.S4, Eq.(S9) the n.d. maximum restoring force exerted on the node by the bistable bearing, F_{bxMax}, Eq.(S10) the n.d. memory bit force profile, F_{bp} plotted in Fig.S4, Eq.(S11) the n.d. nodal displacement associated with generating the maximum restoring force, X_{bFMax}, Eq.(S12) the n.d. characteristic stiffness of the bistable profile, K_{bFmax}, and Eq.(S13) the n.d. bistable equilibrium distance, X_{be}. Scaled displacement, X_{bs}, is defined by normalizing the memory bit displacement, x_b, with respect to the bistable equilibrium distance, x_{be}.

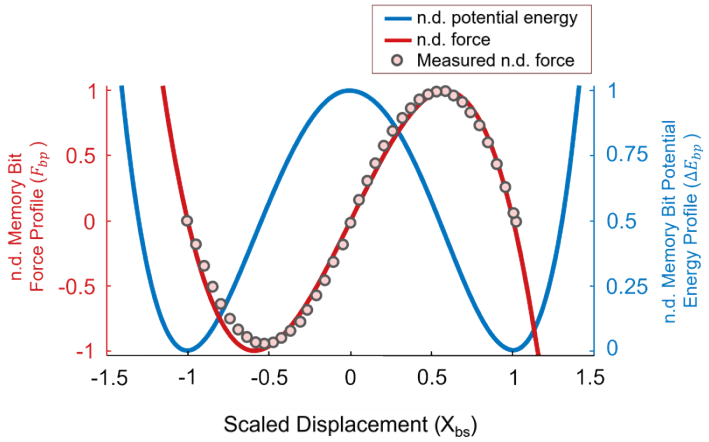

Fig.S4| Simulated force and potential energy profiles of a single memory bit based on the general models. The experimental data exhibit strong agreement with the analytically derived force profile.

$$\Delta E_{bMax} = \frac{\left(2Y_b - \frac{K_{bt}}{1-2R_b}\right)^2}{\left(4-\frac{K_{bt}}{(1-2R_b)^2}\right)} \tag{S5}$$

$$E_{bMin} = Y_b^2 - \Delta E_{bMax} \tag{S6}$$

$$\Delta E_b = E_b - E_{bMin} \tag{S7}$$

$$\Delta E_{bp} = \frac{\Delta E_b}{\Delta E_{bMax}} \tag{S8}$$

$$F_{bxMax} = (1-2R_b)^2\left[\left(4-\frac{K_{bt}}{(1-2R_b)^2}\right)^{2/3} - \left(4-\frac{2Y_b}{(1-2R_b)}\right)^{2/3}\right]^{3/2} \quad \text{(S9)}$$

$$F_{bp} = \frac{F_{bx}}{F_{bxMax}} \quad \text{(S10)}$$

$$X_{bFMax} = \sqrt{1-\left(\frac{4-\frac{2Y_b}{(1-2R_b)}}{4-\frac{K_{bt}}{(1-2R_b)^2}}\right)^{2/3}} \quad \text{(S11)}$$

$$K_{bFMax} = \frac{F_{bxMax}}{X_{bFMax}} \quad \text{(S12)}$$

$$X_{be} = \sqrt{1-\left(\frac{4-\frac{2Y_b}{(1-2R_b)}}{4-\frac{K_{bt}}{(1-2R_b)^2}}\right)^{2}} \quad \text{(S13)}$$

PULSE PROPAGATION

Propagation regimes

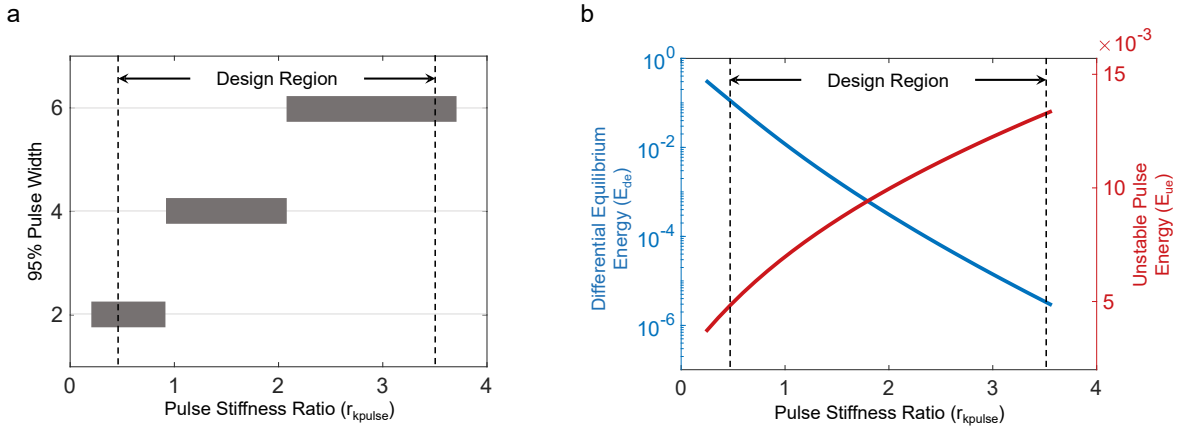

Fig.S5 | Effect of pulse stiffness ratio on pulse behavior. a, The pulse stiffness ratio r_{kPulse} determines the pulse properties. Increasing r_{kPulse} results in higher pulse width. 95% pulse width refers to the number of nodes (in a chain of memory bits with repeated elements) with $|X_{bs,n}| < 0.95$ while the pulse is at UE. **b,** With higher r_{kPulse}, the differential equilibrium energy (E_{de}) decreases, while the unstable pulse energy (E_{ue}) increases. The design region indicates the design range for r_{kPulse}, where pulse energy and pulse width are balanced for effective signal propagation.

The memory bit general model shows signal propagation only occurs in certain compliance regimes. In these regimes, a soliton can propagate along a chain of memory bits (Fig.S5a). We define a decision hierarchy to simplify propagation regime discovery.

First, choose the element energy k_{ba} and size scale l_b, which then determine explicit values for all geometric and stiffness values.

Second, choose the bistable energy storage scale via Y_b, the memory bit axial pre-load compression, as well as the approximate angle of the lever arm at bistable equilibrium, θ_b, via Eq.(S14). Generally, $Y_b \approx 0.2$ is an upper bound as this corresponds to ≈26° rotation, which is large scale motion for compliant bearings.

$$\theta_b \approx \cos^{-1}(1 - Y/2) \tag{S14}$$

Third, choose the compliant bearing approach and set the effective cross-pivot rolling radius R_b to describe the scale of rolling, which occurs in the bearing during large range rotation.

Fourth, choose the transverse stiffness K_{bt}, which modulates the depth of the bistable potential energy well. Ideally, K_{bt} should approach 1 to keep all stiffnesses at the same scale and simplify fabrication, however bistability disappears when $K_{bt} > K_{btMax}$, defined in Eq.(S15). A practical value of $K_{bt} = K_{btMax}/2$ maintains high memory bit stiffness to allow for manufacturing feasibility without suppressing bistability.

$$K_{btMax} = 2Y(1 - 2R_b) \tag{S15}$$

Fifth, and finally, the coupling stiffness K_{bc} is used to engineer the pulse properties, including the propagation speed, pulse size, and pulse energy. The pulse properties are governed by the pulse stiffness ratio, r_{kPulse}, which describes the balance between the n.d. coupling stiffness, K_{bc}, with the n.d. characteristic stiffness of the memory bit profile, K_{bFMax}, via Eq.(S16).

$$r_{kPulse} = \frac{K_{bc}}{K_{bFMax}} \tag{S16}$$

The coupling stiffness captures the ability of nodes to affect neighbors while the characteristic stiffness captures the ability of nodes to resist neighbors. The pulse stiffness ratio r_{kPulse} also captures a lower limit to pulse propagation which occurs when the coupling stiffness is too low to pull the rising node over the peak restoring force.

Consider a chain of N memory bits connected by N-1 coupling linkages. A simple force balance, Eq.(S18) is established for three nodes, [n-1, n, n+1], with nodes n-1 and n+1 approximated at bistable equilibria, $X_{b,n-1} = -X_{b,n+1} = X_{be}$, even though the finite compliance of the chain always results in the node being positioned closer than this. The moving node n is then controlled by the balance of the three dominant forces: (i) the coupling stiffness pulling it to the right from the preceding node n-1 at the positive equilibrium, (ii) the bistable restoring force pulling it back to the left toward the initial negative equilibrium, and (iii) the coupling stiffness of the following node n+1 at the negative equilibrium, as shown in Eq.(S17).

$$\underbrace{(X_{be} + X_{bFMax})K_{bc}}_{n-1} - \underbrace{(X_{be} - X_{bFMax})K_{bc}}_{n+1} - \underbrace{F_{bxMax}}_{n} \geq 0 \tag{S17}$$

The simplified expression compares the coupling stiffness and characteristic profile stiffness in Eq.(S18), producing a simple constraint $r_{kPulse} > ½$ to propagate the pulse.

$$2K_{bc} - K_{bFMax} \geq 0 \tag{S18}$$

By balancing the forces through a chain of repeated bistable memory bit units connected by coupling linkages, Fig. 2c,d and Fig.S6, we developed a model to identify the effect of pulse stiffness ratio variations. A weak r_{kPulse} generates short pulses across few nodes while increasing the pulse stiffness ratio leads to a strong coupling linkage that extends the pulse length towards infinity, shown in Fig.S6a.

Analyzing the pulse energy demonstrates the effect of r_{kpulse} on the pulse. The difference between the n.d. displacement of two adjacent nodes n and n+1, represented by $X_{b,n} - X_{b,n+1}$, signifies the displacement of the coupling linkage connecting these nodes. The n.d. stiffness of this coupling linkage is denoted by $K_{bc,n}$. The total n.d. energy stored in all coupling linkages within a chain of memory bits is defined by Eq.(S19).

$$E_{bc} = \sum_{n} K_{bc,n}(X_{b,n+1} - X_{b,n})^2 \tag{S19}$$

The pulse unstable and stable equilibrium energies, denoted as E_{ue} and E_{se}, represent the total potential energies stored in the pulse in the unstable equilibrium (UE) and stable equilibrium (SE) states, respectively. The total potential energy includes both the potential energy of individual nodes and the energy stored in the coupling linkages between them, as long as their displacements meet the conditions of Eq.(S20) at the pulse SE state.

In the UE state, the central node in the chain shows no displacement. However, in the SE state, there are two central nodes, each displaced equally but in opposite directions. The steady-state displacements of each node at UE, denoted as $X_{ue,n}$, and SE, denoted as $X_{se,n}$, are determined by balancing the forces acting on the nodes. These displacements are then used to define E_{ue} and E_{se} via Eq.(S21) and Eq.(S22).

$$-1 + 5 \times 10^{-7} < X_{bs,n} < 1 - 5 \times 10^{-7} \tag{S20}$$

$$E_{ue} = \sum_{n} K_{bc,n}(X_{ue,n+1} - X_{ue,n})^2 + \sum_{n} (K_{bt} X_{ue,n}^{2} + \left[Y_b - (2 - 4R_b)(1 - \sqrt{1 - X_{ue,n}^{2}})\right]^2) \tag{S21}$$

$$E_{se} = \sum_{n} K_{bc,n}(X_{se,n+1} - X_{se,n})^2 + \sum_{n} (K_{bt} X_{se,n}^{2} + \left[Y_b - (2 - 4R_b)(1 - \sqrt{1 - X_{se,n}^{2}})\right]^2) \tag{S22}$$

The difference between the two pulse energy states is then normalized to derive the equilibrium energy differential, E_{de}, Eq.(S23).

$$E_{de} = \frac{E_{ue} - E_{se}}{E_{ue}} \tag{S23}$$

The energy equilibrium differential approximates the energy cost to advance the pulse by one node (Fig.S6b). At high pulse stiffness ratios, E_{de} falls without limit. Discrete soliton behavior is only clearly observable in the design region r_{kpulse} = [0.5 - 3.5] (Fig.S6a,b). The lower bound occurs when the maximum displacement between adjacent nodes is insufficient to pull the downstream element over its peak restoring force, halting the pulse propagation. The upper propagation bound is practically defined by increasing pulse width and stored energy, which lead to increasingly difficult pulse triggering. Pulse engineering balances tradeoffs between small pulse energy, short travel and compactness (low r_{kpulse}) versus high pulse energy, long travel and wide pulse widths (high r_{kpulse}).

Nodal energy tuning for pulse propagation

Here, we show how the minimum energy step is tuned for each node, resulting in memory bits with the same kinematics but successively less potential energy, thus engineering the pulse chain for pulse propagation. The node 'energy' is calculated as the potential energy of a pulse in UE centered on the node, assuming no energy decrement across the pulse. This allows the measurement to be a spot analysis of the pulse characteristics at the node. The pulse energy profile is engineered by calculating the energy and minimum energy step of the *n*'th nodes. The *n*+1 nodal energy decrements from the *n* node by the minimum energy step. In order to ensure fabrication variation does not halt pulse propagation we scaled by the minimum energy step by a factor of 1.5x, however future work could hone this value. The energy of each node is tuned by adjusting k_{ba} for the memory bit. The process is repeated by calculating the minimum energy step for the *n*+1 node being used to determine the energy of the *n*+2 node and so on.

Potential energy map

A potential energy map (PEM) is defined for the pulse propagation through a single node (Fig.S7). The PEM is captured by tracking the potential energy of a steady state pulse profile as the center node *n* shifts from UE arrangement, q, where $x_{b,n}$ = 0, to the SE, and to the next UE arrangement, q+1, where the pulse center is at node n+1, $x_{b,n+1}$ = 0 and node n is off center at the next UE

displacement, $x_{b,n} = x_{ue1}$. This represents the transition of the pulse center from node *n* to node *n*+1. At SE, the pulse center lies between two nodes with equal displacements but opposite signs, $|x_{b,n}| = |x_{b,n+1}| = x_{se1}$, Fig.S6.

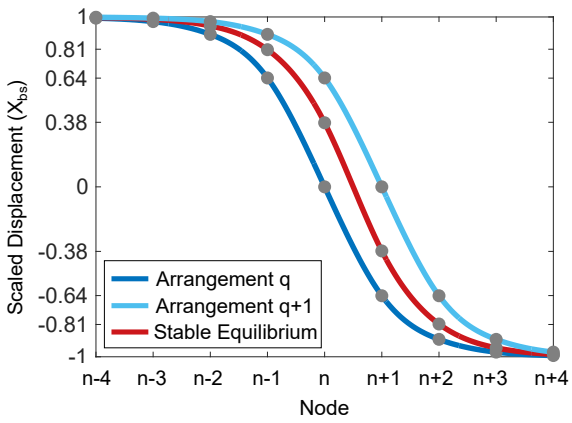

Fig.S6 | Stable vs Unstable equilibrium. The plot illustrates scaled displacement of each node in a chain of repeated bistable memory bits in both stable (red line) and unstable (blue lines) equilibrium states. The steady-state displacements are determined by balancing forces acting on the nodes. In the stable equilibrium state, the pulse center is positioned between two nodes, specifically between nodes n and n+1 in this case. In the unstable equilibrium state, the pulse center is located on a single node, shown here as node n in arrangement q and node n+1 in arrangement q+1.

PEM insight is gained by tracking the dynamic energy flows through the pulse by calculating the pulse energy while the center node n moves from arrangement q, $x_{b,n} = 0$, to arrangement q+1, $x_{b,n} = x_{ue1}$, in *i* identical displacement steps of amount *dx*, $x_{ue1} = i.dx$.

The change in kinetic energy per step, $e_{k,i} - e_{k,i-1}$, is balanced by the energy dissipated per step, $de_{d,i}$, and the potential energy change per step, $e_{p,i} - e_{p,i-1}$, shown in Eq.(S24).

$$(e_{k,i} - e_{k,i-1}) + de_{d,i} + (e_{p,i} - e_{p,i-1}) = 0 \tag{S24}$$

The potential energy is calculated using the UE pulse profile. While the pulse profile shifts from the unstable to stable and back to unstable equilibrium, it is simpler to approximate as a single profile energy value as the profiles produce nearly identical results. The pulse profile does not have uniform velocity as the center shifts. Rather, the nodes at the center have higher velocity than those at the edge. The velocity profile, $\Delta x_{ue,n}$, can be defined via 'ΔX per node advance of the pulse' and measured by finding the distance each node must traverse when pulse center moves one node forward, i.e. from arrangement q to q+1, Eq.(S25).

$$\Delta x_{ue,n} = (x_{b,n})_{q+1} - (x_{b,n})_q \tag{S25}$$

The velocity profile is normalized to the maximum velocity in pulse advance, center node displacement when the pulse moves one node forward, $\Delta x_{ue,n\,=\,center\ node} = x_{ue1}$. The normalized velocity profile provides a scaling factor for each node's velocity relative to the velocity of the center node in each step, a value which is set by v_i for each step. The assumption that the tracked node location is always at the peak velocity is acceptable since the PEM is analyzed for small displacements around $X_b = 0$ where the tracked node is on the plateau of high velocity at the center of the pulse profile. The kinetic energy is then the sum of all these velocities for the *i*'th step, as shown in Eq.(S26).

$$e_{k,i} = \frac{1}{2} m_b v_i^2 \sum_n \left(\frac{\Delta x_{ue,n}}{x_{ue1}}\right)^2 \tag{S26}$$

The dissipated energy is a product of the damping coefficient c_b, the average nodal velocity over the course of each displacement step, dx, and the distance traveled by each node over the course of the step as shown in Eq.(S27). Both the velocity and distance must be normalized by the pulse velocity profile.

$$de_{d,i} = c_b dx \frac{v_i + v_{i-1}}{2} \sum_n \left(\frac{\Delta x_{ue,n}}{x_{ue1}}\right)^2 \tag{S27}$$

The pulse potential energy as a function of center node location is extrapolated as a sinusoidal variation between pulse energy at unstable equilibrium, e_{ue}, and stable equilibrium, e_{se}. While this is a simplification of the actual profile, the scale of energy variation was found to be small and locally flat around the equilibria, so the sinusoidal profile worked well as an approximation. A linear slope was added to the approximation to capture the slight decrement in nodal energy by e_{step} per node down the chain, shown in Eq.(S28).

$$e_{p,i} = \begin{cases} (e_{ue} - e_{se}) \dfrac{\cos\left(\pi \dfrac{idx}{x_{se1}}\right) - 1}{2} - e_{step} \dfrac{idx}{x_{ue1}} & if \quad idx < x_{se1} \\ (e_{ue} - e_{se}) \dfrac{-\cos\left(\pi \dfrac{idx - x_{se1}}{x_{ue1} - x_{se1}}\right) - 1}{2} - e_{step} \dfrac{idx}{x_{ue1}} & if \quad x_{se1} \le idx \le x_{ue1} \end{cases} \tag{S28}$$

All terms are gathered using Eq.(S24) and rearranged around the unknown parameter, v_i, into a second order polynomial shown in Eq.(S29) which can be solved using the quadratic formula for the pulse velocity at each displacement step, *i*.

$$\left[\frac{1}{2} m_b \sum_n \left(\frac{\Delta x_{ue,n}}{x_{ue1}}\right)^2\right] v_i^{\,2} + \left[\frac{c_b dx}{2} \sum_n \left(\frac{\Delta x_{ue,n}}{x_{ue1}}\right)^2\right] v_i \ldots + \left[e_{p,i} - e_{p,i-1} + \frac{c_b dx}{2} \sum_n \left(\frac{\Delta x_{ue,n}}{x_{ue1}}\right)^2 v_{i-1} - e_{k,i-1}\right] = 0 \tag{S29}$$

The n.d. critical energy for pulse propagation is defined as $E_{min} = \dfrac{e_{min}}{e_{ue}}$, where e_{min} is the minimum value of e_{step} at which $v_i > 0$ over the full range of the PEM. The energy is a complex combination of kinetic and potential effects so does not lend itself to a simple analytical expression.

The pulse eventually settles into a local stable equilibrium if the potential energy step between each memory bit nodes in a chain, $E_{step,}$ is 0. Pulse propagation is only possible if the gate characteristic energy is successively decremented for each downstream node. Inter-node step energy must be sufficiently low, $E_{step}=E_{min}$, for the soliton kinetic energy to reach the next SE state. With each nodal advance, the pulse potential energy transforms into kinetic energy. For practical operation given manufacturing variability, $E_{step}=1.5E_{min}$ ensures the step energy is consistently above the minimum threshold (Fig.S7).

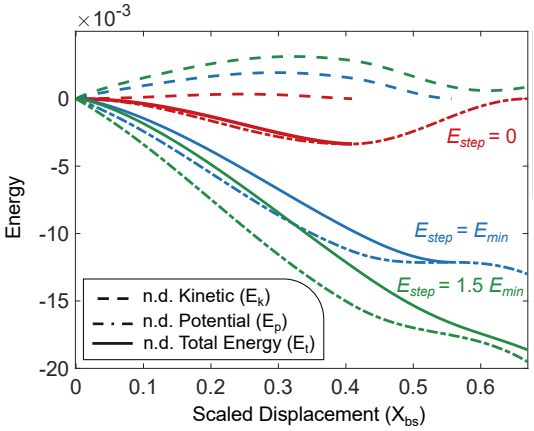

Fig.S7 | Pulse energy map (PEM). The normalized pulse potential energy map (PEM) between successive unstable equilibria UE peaks, across a bistable bit displacement from 0 <X_{bs}< 0.64, shows non-propagating state E_{step} = 0, critical energy E_{step} = E_{min}, and propagating energy E_{step} = 1.5 E_{min}.

To design a chain of bistable nodes capable of signal propagation, Eq.(S30) should be satisfied while keeping all nondimensionalized geometric parameters constant.

$$k_{ba,n+1} = (1 - E_{step})k_{ba,n} \tag{S30}$$

Pulse propagation – steady state velocity

A pulse propagates along a memory bit chain at an approximately steady state velocity, determined by the energy flow from the pulse potential energy into energy dissipation e_d, where the unknown is the time increment for the pulse to advance one node, dt. The velocity of the n'th node in the profile $\Delta x_{ue,n}/dt$, and the distance each node travels $\Delta x_{ue,n}$, are used to calculate the dissipated energy, Eq.(S31).

$$e_d = c_b \sum_n \frac{\Delta x_{ue,n}}{dt} \Delta x_{ue,n} = e_{step} \tag{S31}$$

The known energy decrement between nodes, e_{step}, leads to the time increment between nodes, Eq.(S32).

$$dt = \frac{c_b}{e_{step}} \sum_n (\Delta x_{ue,n})^2 \tag{S32}$$

AND GATE

AND gate kinematic design

Fig.S8 shows the detailed structure of the AND gate, composed of several linkages, which freely rotate relative to one another with cross-pivot flexural hinges. The l_{a1}, l_{a2} linkages from the input ports to the first rotary joint are structured in a V to allow for the two input ports to expand away from one another along the Y-axis. The V ensures the structure does not lock when it rotates, since the rotation moves l_{a1} to increase slightly when the input ports are guided by linear shuttles. The AND gate inputs and output are connected to memory bits, which kinematically constrain the AND gate shuttle motion. The memory bits are connected on separate levels, however right-angle linkages could maintain an alternative planar design. Rigid linkages provide high transverse stiffness to reject unwanted state changes via back-driving. Compressive compliance at the AND gate output is a compliant coupling to enable propagation, analogous to the inter-node compliance in the bistable chain. The AND gate kinematics are initially tuned based on the assumption that the two inputs reach the full equilibrium location, however these displacements are attenuated by finite compliance of the structure and coupling linkages. The central AND gate lever arms are modified beyond the static operation constraint to compensate for this effect and ensure full output propagation despite incomplete input state transitions.

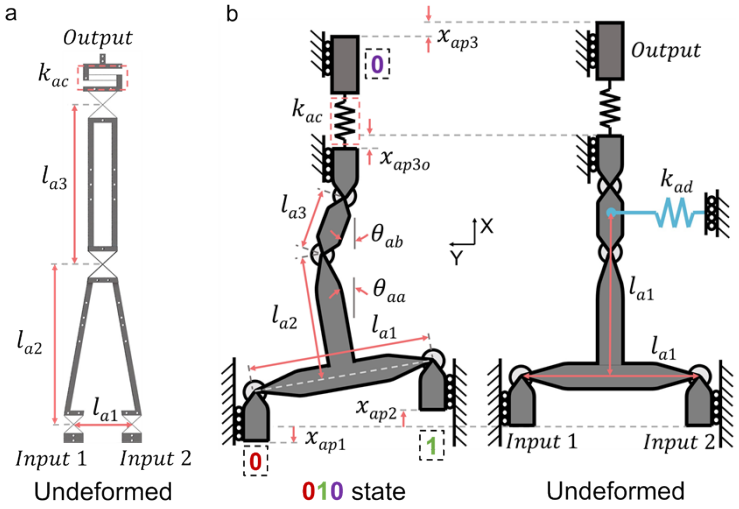

Fig.S8 | AND gate design and pseudo-rigid body model a, Top view of undeformed AND gate CAD. **b,** AND gate parameters mapped to generalized structure in 010 and undeformed states. k_{ad} is an equivalent stiffness representing stiffness of AND gate linkages in a differential motion.

A five-dimensional design space, three geometric l_{a1}, l_{a2} and l_{a3} and two stiffness parameters k_{ad}, k_{ac}, represent the AND gate, where only a small regime enables pulse propagation. Kinematic analysis ensures the rotational nonlinearity produces AND operator performance in ideal conditions. An additional parameter captures the energy transfer behavior of the AND gate, r_{aE}, which describes the ratio of the pulse energy out of the gate, e_{aOut}, compared to the theoretical maximum energy output, $e_{aOutMax}$. Eq.(S34) shows the n.d. terms. The n.d. differential motion stiffness, K_{ad}, is normalized to the compressive stiffness, simplifying elasto-mechanic calculations. The n.d. compressive stiffness, $K_{ac,}$ is normalized to the first coupling linkage stiffness after the output port, k_{acp3}, as this output port stiffness determines the compressive stiffness requirements. All displacements in the AND gate, x_a = [x_{ap1}, x_{ap2}, x_{ap3}, x_{ap3o}, x_{ad}, x_{ac}, x_{as}] and linkage lengths l_a = [l_{a1}, l_{a2}, l_{a3}] are normalized by the equilibrium displacement of the memory bits, x_{be}. Refer to nomenclature for additional details.

The lever arm lengths, l_{a1}, l_{a2}, and l_{a3}, are set by the requirements to ensure AND gate nonlinear behavior as well as the design maximum values set for the two linkage angles, θ_{aaMax}, θ_{abMax}. The stiffness and energy terms, K_{ad}, K_{ac}, and r_{aE}, are set by the requirements of pulse propagation. The AND gate nonlinear response to the two inputs (*p1* and *p2*) is captured in the output port (*p3*) uncompressed displacement, x_{ap3o}.

The input motion X_{ap1}, X_{ap2}, is redefined as differential, X_{ad}, and shared, X_{as}, terms, shown in Eq.(S33) and Eq.(S34).

$$X_{as} = \frac{X_{ap1} + X_{ap2}}{2} \tag{S33}$$

$$X_{ad} = X_{ap2} - X_{ap1} \tag{S34}$$

Eq.(S35) determines the compression displacement X_{ac} by comparing the output motion, X_{ap3} to the uncompressed displacement, X_{ap3o}.

$$X_{ac} = X_{ap3} - X_{ap3o} \tag{S35}$$

Eq.(S36) demonstrates the uncompressed displacement, calculated geometrically, and determined by the differential and shared motion.

$$X_{ap3o} = X_{as} + L_{a2}\left(\sqrt{1 - \left(\frac{X_{ad}}{L_{a1}}\right)^2} - 1\right) + L_{a3}\left(\sqrt{1 - \left(\frac{L_{a2}X_{ad}}{L_{a1}L_{a3}}\right)^2} - 1\right) \tag{S36}$$

The AND gate nonlinear behavior constrains the output port to the same location, regardless of the input port states such that the 000 and 010 states are equivalent. Three constraints are supplied to set the three AND gate linkage sizes when the nonlinear behavior constraint is combined with the design maximum values set for the two linkage angles, θ_{aaMax}, θ_{abMax}. The requirement on the horizontal linkage L_{a1} is simply constrained by the θ_{aa} rotation angle, shown in Eq.(S37).

$$L_{a1} = \frac{2}{sin\theta_{aaMax}} \tag{S37}$$

The requirements on L_{a2} Eq.(S38) and L_{a3} Eq.(S39) capture the nonlinear complexity.

$$L_{a3} = \frac{\dfrac{1}{\sqrt{\dfrac{1}{L_{a1}^2\left(\sqrt{\dfrac{1}{4} - L_{a1}^{-2}} - \dfrac{1}{2}\right) + 1} + L_{a1}^2 - 2}} + \dfrac{[\cos\theta_{abMax}]^{-1}}{\dfrac{1}{L_{a1}\left(\sqrt{\dfrac{1}{4} - L_{a1}^{-2}} - \dfrac{1}{2}\right)} + L_{a1}} + \tan\theta_{abMax}}{\tan\theta_{abMax}[2 + L_{a1} sin\,\theta_{abMax}]} \tag{S38}$$

$$L_{a2} = \frac{1}{2}\sqrt{\frac{1 - 2L_{a3}}{L_{a1}^2\left(\sqrt{\dfrac{1}{4} - L_{a1}^{-2}} - \dfrac{1}{2}\right) + 1} + L_{a3}^2} + \frac{1}{2} - \frac{L_{a3}}{2} \tag{S39}$$

The next design steps define gate elastomechanics based on the two internal stiffnesses. The force of the AND gate on each port's node, $f_a = [f_{ap1}, f_{ap2}, f_{ap3}]$ is defined in each case as positive in the +x-axis direction and nondimensionalized to $F_a = [F_{ap1}, F_{ap2}, F_{ap3}]$ by the characteristic gate force, $k_{ac}x_{be}$, as shown in Eq.(S40).

$$F_a = \frac{f_a}{k_{ac}x_{be}} \tag{S40}$$

Differential stiffness between the input ports generates equal and opposite forces on the input gates, while compression stiffness generates a return force, modified by gate kinematics, captured by the term α_{aF} as shown in Eq.(S41).

$$\alpha_{aF} = \frac{L_{a2}X_{ad}}{L_{a1}^2}\left[\left[\left(\frac{L_{a3}}{L_{a2}}\right)^2 - \left(\frac{X_{ad}}{L_{a1}}\right)^2\right]^{-\frac{1}{2}} + \left[1 - \left(\frac{X_{ad}}{L_{a1}}\right)^2\right]^{-\frac{1}{2}}\right] \tag{S41}$$

Eq.(S42) is the nodal force at the first input port, F_{ap1}.

$$F_{ap1} = K_{ad}X_{ad} + \left(\frac{1}{2} + \alpha_{aF}\right)X_{ac} \tag{S42}$$

Eq.(S43) is the nodal force at the second input port, F_{ap2}.

$$F_{ap2} = -K_{ad}X_{ad} + \left(\frac{1}{2} - \alpha_{aF}\right)X_{ac} \tag{S43}$$

Eq.(S44) is the nodal force at the output port, F_{ap3}.

$$F_{ap3} = -X_{ac} \tag{S44}$$

Signal propagation through the AND gate is determined by several stiffness and energetics terms. The maximum differential stiffness, k_{adMax}, is defined by the total energy flow of the pulse into charging the differential mode accounting for the energy lost to dissipation during the traversal of the pulse between nodes, e_{aDis}, and the minimum value of the pulse energy at the inputs, e_{aIn}, as shown in Eq.(S45).

$$k_{adMax} = \frac{e_{aIn} - e_{aDis}}{2x_{be}^2} \tag{S45}$$

The differential stiffness ratio r_{kad} captures the extent to which the pulse energy is routed to the differential mode as shown in Eq.(S46). Fig.3h shows that high efficiency AND gates exist in the $r_{kad} = 0.15$ regime, where only 15% of the pulse energy is drained to the differential mode.

$$r_{kad} = \frac{k_{ad}}{k_{adMax}} \tag{S46}$$

The energy ratio, r_{aE}, is the ratio of the output energy over the available energy after accounting for losses. The energy ratio determines the pulse energy at the gate output, generally set around 0.8 to ensure propagation despite fabrication variation, and the theoretical maximum energy output of the gate, $e_{aOutMax}$, calculated as shown in Eq.(S47). The theoretical maximum energy

output considers energy dissipation and energy storage in the differential mode. The theoretical maximum energy output value provides an energetics-based system constraint, but it is often not the limiting factor.

$$e_{aOut} = r_{aE} \underbrace{e_{aOutMax}}_{(e_{aIn} - e_{aDis} - 2k_{ad}x_{be}^2)} \tag{S47}$$

AND gate efficiency

The overall gate efficiency, η_a, is the ratio of the gate energy output, e_{aOut}, over input, e_{aIn}, and thus will always be a lower than r_{aE}. Kinematic modifications are necessary to ensure propagation, as the preceding analysis assumes all ports are at the bistable equilibrium locations. Tuning a parameter, such as l_{a1}, to overcompensate the gate output ensures the incomplete input transitions still produce sufficient output displacement to drive pulse propagation. In this work, l_{a1} is the preferred term for modification and is slightly reduced to amplify the gate response to input motions. All nodes in the profile are then displaced beyond the threshold $x_{trans}/x_{be} \approx 0.98$ to add less energy to the profile than lost by nodal advancement. Propagation switches from energetically unfavorable to favorable once the output node passes the threshold. The AND gate static force balance captures the unstable equilibrium when the output port reaches the transition displacement, accounting for the input ports being connected to the tail end of a pulse profile rather than locked at equilibrium displacements. Eq.(S48) shows where functions $f_{bxp1}(\ldots)$, $f_{bxp2}(\ldots)$ are the nodal memory bit forces at the input 1 and 2 locations; $f_{ap1}(\ldots)$, $f_{ap2}(\ldots)$ and $f_{ap3}(\ldots)$ are functions calculating the nodal AND gate forces at the input 1, 2 and output; k_{cp1} and k_{cp2} are the coupling stiffnesses of the linkages to the input 1 and 2 ports; The coupling stiffness scaling terms account for the extended chain of nodes connected to the port node. The stiffnesses k_{bxp1} and k_{bxp2} are the memory bit bearing stiffnesses of the input 1 and 2 ports. We assume the output port node experiences no forces from the chain, since forces on the output port switch direction, passing through 0 during transition. The modified l_{a1} term is extracted from the system of equations, producing the value used in the fabricated AND gate to ensure pulse propagation.

$$\begin{aligned}
&given\ x_{ap3} = x_{trans} \\
&k_{cp1}(-x_{be} - x_{ap1})\left(1 - \frac{k_{cp1}}{2k_{cp1} + k_{bxp1}(x_{be})}\right) + f_{bxp1}(x_{p1}) + f_{ap1}(x_{ap1}, x_{ap2}, x_{ap3}, l_{a1trans}) = 0 \\
&k_{cp2}(x_{be} - x_{ap2})\left(1 - \frac{k_{cp2}}{2k_{cp2} + k_{bxp2}(x_{be})}\right) + f_{bxp2}(x_{ap2}) + f_{ap2}(x_{ap1}, x_{ap2}, x_{ap3}, l_{a1trans}) = 0 \\
&f_{ap3}(x_{ap1}, x_{ap2}, x_{ap3}, l_{a1trans}) = 0 \\
&find\ x_{ap1}, x_{ap2}, l_{a1trans} \rightarrow l_{a1trans}
\end{aligned} \tag{S48}$$

Circuit synthesis

The AND gate chain in Fig.4a, b, c used the following parameters: Y_b = 0.1, K_{bt} = 0.065, K_{bc} = 0.063, initial k_{ba} = 32789 N/m, l_b = 35mm, and E_{step}/E_{min} =1.5, which produced a 1.96% energy drop per node. The AND gate was designed with maximum angular deviation for θ_a, θ_b = 10°, r_{kad} = 0.15 which produced k_{ad} = 154N/m, k_{ac} = 1876N/m, l_{a1} = 108.6mm, l_{a2} = 322.2mm, l_{a3} = 322.2mm. The mass of the bistable element stage was 0.2470 kg, with a n.d. damping ratio of 0.034. The mass of the AND gate was 3.507 kg. The bistable element chain in Fig.4d, e, f used the following parameters: Y_b = 0.1, K_{bt} = 0.065, K_{bc} = 0.06, initial k_{ba} = 37643 N/m, l_b = 35mm, E_{step}/E_{min} =1.5, which produced a 1.96% energy drop per node. These simulation parameters were estimated from measurements of the hardware and tuned based on the experimental data.

EULERIAN DYNAMICS MODEL

The dynamic simulation implemented in MATLAB™ begins by initializing the simulation data parameters for each nodal position, velocity, acceleration as well as the kinetic and potential energies of the nodes and couplings in arrays. A separate array indicates the connections between the nodes representing both memory bits and the AND gate. In future work to extend this to additional gate designs such as NOT, OR, NAND etc they could also be represented by nodes with specific dynamics such as demonstrated in the AND gate characterization. The simulation uses the initial estimates for the position, velocity and acceleration as well as any inputs and then calculates a force balance on each node. These results define the 'Pulse Energy Map' as a pulse travels through a node. The pseudo-rigid body models for the memory bits shown in Figure 2a, Figure S1 and for the AND gate in Figure 3a and Figure S8 show the geometric measurements, stiffness, and compliance for each component in the circuit.

Macro-fabrication

The macroscale gates in Fig.4a and Fig.4d were fabricated using wire EDM in Aluminum 7075 T. There were two base gate designs A and B for the top and bottom cross-pivot flexures, offset using acrylic. To achieve an energy decrement along the chain the axial stiffness and the transverse stiffness were tuned for each gate. The axial stiffness was tuned by adding modular stacks of parallel blade flexures. The transverse stiffness was modulated using 0-degree of freedom wave springs to add stiffness without adding constraints.

Alternate Circuit Designs

Other circuits can be created using the basic elements described in this work. Several addition elements are presented in Fig.S9 to aid in circuit development, including 90° turns in Fig.S9a, 180° turns in Fig.S9b, and a NOT gate in Fig.S9c. The AND and NOT gates are a logically complete set of gates, meaning all possible logical operations can be formed from these elements.

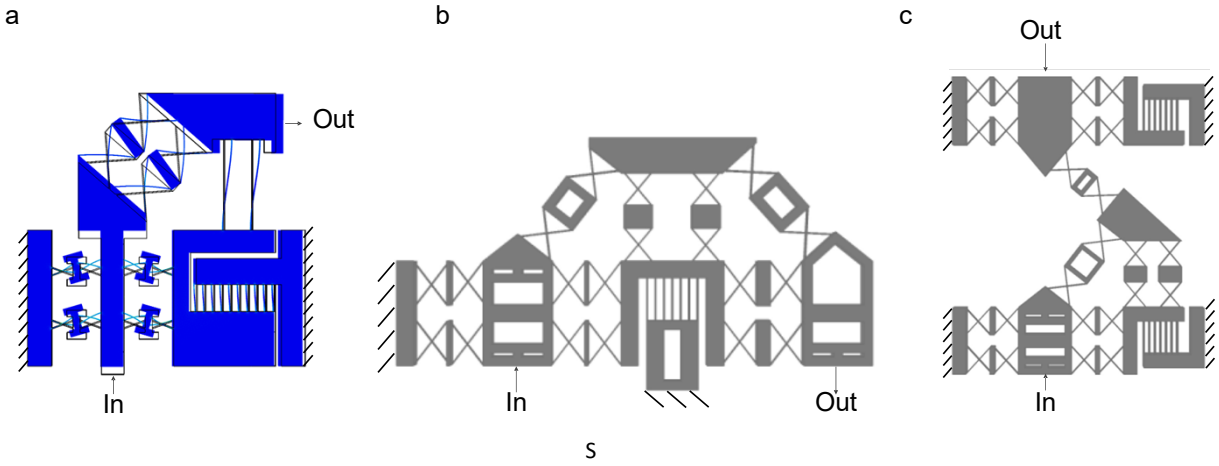

S

Fig.S9 | Complex circuits require combinations of logic elements. a, A 90° turn for circuit routing. **b,** A 180° full turn. **c,** A NOT gate paired with an AND gate is a complete set of logical operations.

Microfabrication

Two-photon lithography (TPL)[3,4] is a microscale additive manufacturing method that enables rapid prototyping of micro mechanisms. TPL occurs when two photons are absorbed at the same time to activate a photo-initiator molecule and it requires a high flux of photons both locally and temporally. The photons are focused tightly by a high numerical aperture objective lens and are compressed in ultra-short pulses using a femto-second pulsed laser. By satisfying these two conditions the non-linear TPL process takes place with higher resolution compared to conventional laser lithography methods.

The custom TPL system (Fig.S10) used to fabricate the microscale structures in this research is composed of a tunable wavelength femtosecond pulsed laser (fs laser, SpectraPhysics MaiTai eHP DS), an acousto-optic modulator (AOM, IntraAction ATM-802DA2) combined with a mirror (M) and beam block (BB), which act as a high speed beam shutter and also a power controller, a beam expander system (BE), 2D mirror galvanometers (Galvo, Thorlabs GVS012) that scan the beam in the x-y plane at the fabrication site, a 4-F telescope relay, a dichroic mirror (DM), a 100X microscope objective (MO, Olympus Plan Apo Lambda, NA = 1.45), a dichroic filter (DF), a z-axis piezo objective scanner with 600µm travel range (MO scanner, Thorlabs PFM450E), a 3-axis micro positioning stage (Stage, Thorlabs RB13M), a light emitting diode source (LED, Thorlabs M617L3), and a camera (40X cam, Basler ace acA1300-75gm) connected to a custom 40X magnification imaging tube including a tube lens (TL) and two lenses (L).

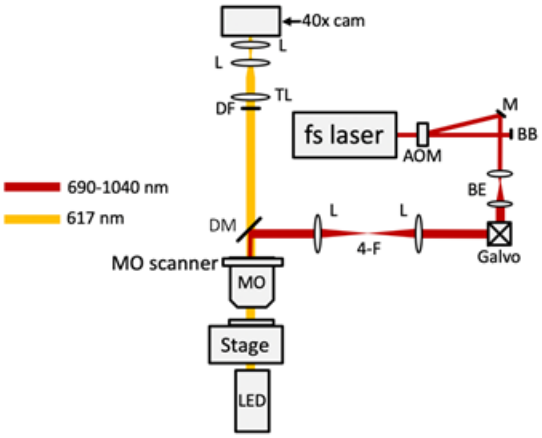

Fig.S10 | A schematic of the two-photon lithography system.

To overcome low adhesion between the polymer and the glass substrate, a chemical functionalization procedure was conducted:

1) O2 plasma treatment for three minutes on the substrate.
2) Substrate immersion in a solution of anhydrous ethanol (93 vol%), deionized water (5 vol%), and 3-acryloxypropyl trimethoxysilane (2 vol%) for 16 hours.
3) Substrate immersion in anhydrous ethanol for 1 hour.
4) Baking at 95°C for 1 hour.

Nanoscribe IP-Dip is used as the photocurable polymer to fabricate the structures. In this work, the average laser scanning speed was 1 mm/s and the beam power was set to be 90 mW at 780 nm, measured before the objective.

The TPL system working area is 250 µm by 250 µm, thus to fabricate the AND gate and the chain of memory bits (Fig.5), neighboring elements are printed individually and then stitched together. Spacing is precisely controlled with alignment marks. The printed structures are post processed by washing away the uncured photopolymer using propylene glycol methyl ether acetate (PGMEA) immersion for 13 minutes followed by isopropyl alcohol (IPA) immersion. Throughout the testing procedure, the structures are kept submerged in IPA to avoid the undesired effects of surface tension forces on the microstructures caused by evaporation.

All microscale designs are mechanically supported by three grounded regions on the glass substrate (Fig.S11). The out of plane thickness of the elements in Fig.S11 is 36µm, and the overhanging structures are printed at 12 µm clearance from the substrate.

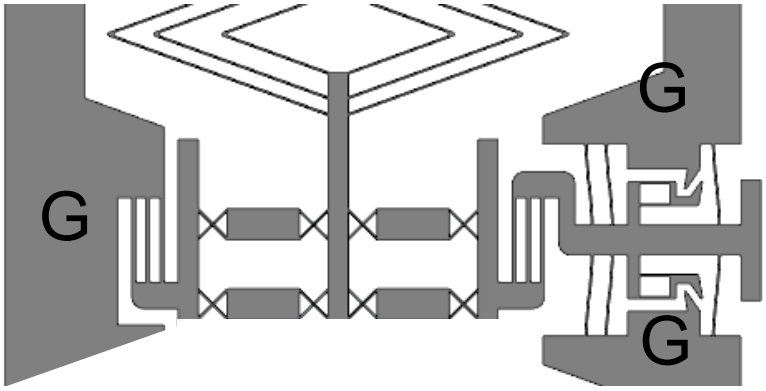

Fig.S11 | Top view of a single bistable bit design. The tabs shown with "G" are grounded to substrate. All other features are overhanging.

Sequential Micro Fabrication

The sequential printing method enables additive manufacturing of large overhanging features without supports using two-photon lithography (TPL). To print the model shown in Fig.S12, the overhanging geometries are divided into shorter substructures to reduce unwanted layer movement while printing and to increase the precision and quality of fabricated structures. The sub-structures are printed in a specific order to ensure each printed feature is connected to a previously grounded or stable structure. The maximum layer height of substructures is limited to 12µm to avoid obscuring the TPL laser beam in the subsequent printing of features located on the lower layers.

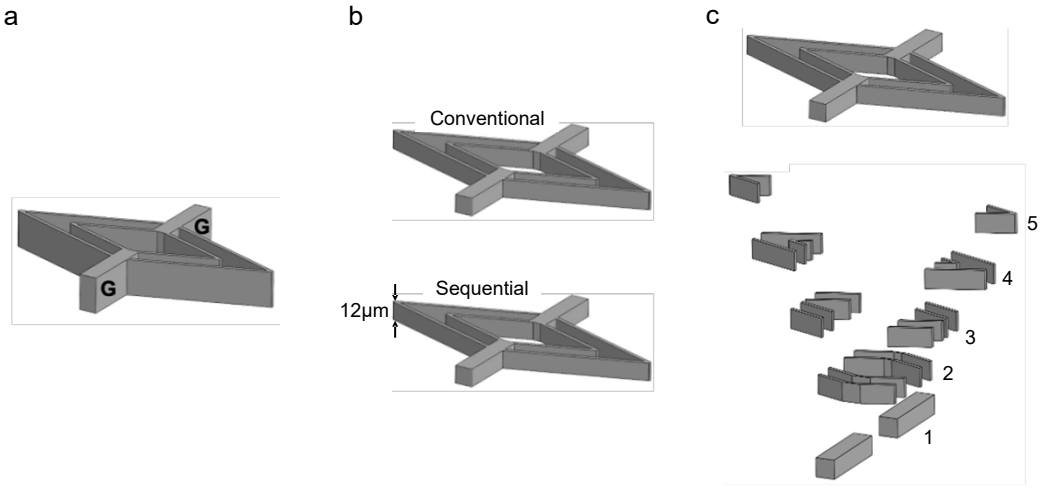

Fig.S12 | Sequential printing approach. **a**, A coupling linkage geometry grounded only at specific features denoted "G," with the rest of the structure overhanging. **b**, The bottom 12 µm of the structure is separated and printed using the sequential method, as labeled. The rest of the structure is printed on top using the conventional layer-by-layer method. **c**, The bottom portion of the structure, with a proposed maximum thickness of 12 µm, is decomposed into smaller overhanging pieces that are printed in 5 steps. First, the grounded portions are printed, followed by the addition of features in step 2, and continuing in sequence until step 5. Printing short, cantilevered sections instead of longer overhangs results in a stiffer structure, reducing unwanted motion and increasing layer alignment precision. Once the foundation is established using this method, the structure can be grown in the z-direction using the conventional layer-by-layer method to achieve the desired feature height.

Nomenclature

Symbol	Name	Definition	Other forms
Bistable memory bit (MB)			
r_b		Effective rolling radius	$R_b = \frac{r_b}{l_b}$
l_{bf}		Cross-pivot flexure length	
a	Instant center location	Location of the instant center of rotation normalized to the flexure length	
θ_{bf}	Cross-pivot angle	Angle between the cross-pivot flexures, typically $90°$	
l_b	Lever arm characteristic length	Sets element geometrical size scale, used to nondimensionalize displacements or lengths related to a single memory bit	
k_{ba}	MB axial stiffness	Intra-element, characteristic stiffness of the memory bit in the Y direction, perpendicular to signal propagation. Tunes memory bit energy scale.	
y_b	Y-axis displacement	Displacement from pre-load	$Y_b = \frac{y_b}{l_b}$
k_{bt}	MB transverse stiffness	Intra-element memory bit stiffness in the X direction, parallel to signal propagation. Accesses bistable behavior by modulating the potential energy. Optimal transverse stiffness is dependent on compression distance and flexure performance.	$K_{bt} = \frac{k_{bt}}{k_{ba}}$
x_b	x-axis displacement	Displacement of a memory bit in the X direction. $x_{b,n}$ refers to the x-axis displacement of node n in a chain of memory bits.	$X_b = \frac{x_b}{l_b}$
X_b	n.d. displacement	n.d. displacement of a memory bit in the X direction.	
k_{bc}	MB coupling stiffness	Inter-element stiffness, captures the ability of nodes to affect neighbors.	$K_{bc} = \frac{k_{bc}}{k_{ba}}$
e_{char}	MB characteristic energy	This energy is used to normalize other energy terms of a single memory bit, $e_{char} = \frac{1}{2} k_{ba} l_b^2$	
E_b	MB potential energy	n.d. total potential energy of a single memory bit.	$E_b = \frac{e_b}{e_{char}}$
F_{bx}	MB force	n.d. force generated by the memory bit bearing on the node in the X direction	$F_{bx} = \frac{f_{bx}}{k_{ba} l_b}$
K_{bx}	MB stiffness	n.d. stiffness of the memory bit bearing on the node in the X direction	$K_{bx} = \frac{k_{bx}}{k_{ba}}$
ΔE_{bMax}		n.d. scale of the potential energy change from bistable equilibrium to unstable equilibrium	$\Delta E_{bMax} = \frac{\Delta e_{bMax}}{e_{char}}$
E_{bMin}		n.d. minimum potential energy at bistable equilibrium	$E_{bMin} = \frac{e_{bMin}}{e_{char}}$
ΔE_b		n.d. relative memory bit potential energy	$\Delta E_b = \frac{\Delta e_b}{e_{char}}$

F_{bxMax}	Max bistable force	n.d. maximum restoring force exerted on the node by the memory bit in the X direction	$F_{bxMax} = \frac{f_{bxMax}}{k_{ba} l_b}$
ΔE_{bp}	n.d. MB potential energy profile	Normalized potential energy of a single memory bit	
F_{bp}	n.d. MB force profile	Normalized force of a single memory bit	
X_{bFMax}		n.d. nodal displacement associated with generating the maximum restoring force	$X_{bFMax} = \frac{x_{bFMax}}{l_b}$
K_{bFmax}	Characteristic MB stiffness	The average non-dimentionalized memory bit stiffness over the course of moving from unstable equilibrium position ($X = 0$) to X_{bFMax}.	$K_{bFmax} = \frac{k_{bFMax}}{k_{ba}}$
X_{be}	n.d. bistable equilibrium distance	n.d. displacement of a memory bit at stable equilibrium state.	$X_{be} = \frac{x_{be}}{l_b}$
X_{bs}	Scaled displacement	Defined by normalizing the memory bit displacement, x_b, with respect to the bistable equilibrium distance, x_{be}. $X_{bs,n}$ refers to the scaled displacement of node n in a chain of memory bits. $X_{bs,n}$ refers to the x-axis scaled displacement of node n in a chain of memory bits.	
θ_b	Lever arm angle	Angle of memory bit lever arm	
K_{btMax}		n.d. maximum transverse stiffness. Bistability disappears when $K_{bt} > K_{btMax}$	$K_{btmax} = \frac{k_{btMax}}{k_{ba}}$
Pulse Energy			
r_{kPulse}	Pulse stiffness ratio	n.d. coupling stiffness K_{bc} by the characteristic memory bit stiffness K_{bFmax}. A weak pulse stiffness ratio generates short pulses across few nodes while increasing the pulse stiffness ratio leads to a strong coupling linkage that extends the pulse length towards infinity.	
E_{bc}		n.d. total energy stored in all coupling linkages within a chain of memory bits	$E_{bc} = \frac{e_{bc}}{e_{char}}$
E_{ue}	Unstable pulse energy	n.d. total potential energy stored in all memory bits and the coupling linkages connecting them in a chain of memory bits while the pulse is in UE.	$E_{ue} = \frac{e_{ue}}{e_{char}}$
E_{se}	Stable pulse energy	n.d. total potential energy stored in all memory bits and the coupling linkages connecting them in a chain of memory bits while the pulse is in SE	$E_{se} = \frac{e_{se}}{e_{char}}$
E_{de}	n.d. differential equilibrium energy	Approximates the energy cost to advance the pulse by one node	$E_{de} = \frac{e_{de}}{e_{char}}$
$X_{ue,n}$		n.d. steady-state displacements of node n at UE	$X_{ue,n} = \frac{x_{ue,n}}{x_{be}}$
$X_{se,n}$		n.d. steady-state displacements of node n at SE	$X_{se,n} = \frac{x_{se,n}}{x_{be}}$
x_{ue1}		Center node displacement when pulse shifts from one UE arrangement to the next	

x_{se1}		At SE, the pulse center lies between two nodes with equal displacements of x_{se1}	
Arrangement q		A configuration in which the pulse is in UE, with its center located on node n.	
Arrangement q+1		A configuration in which the pulse is in UE, with its center located on node n+1.	
i	Node step index	Step index which tracks node n motion from arrangement q to q+1.	
dx		Center node n moves from arrangement q to arrangement q+1 in *i* identical displacement steps of amount *dx.*	
$e_{k,i}$		Total pulse kinetic energy at displacement step i	
E_k	n.d. kinetic energy	n.d. total kinetic energy of pulse	$E_k = \frac{e_k}{e_{ue}}$
$e_{p,i}$	potential energy	Total pulse potential energy at displacement step i	
E_p	n.d. potential energy	n.d. total potential energy of pulse	$E_p = \frac{e_p}{e_{ue}}$
E_t	n.d. total energy	n.d. total pulse energy including kinetic and potential energies	$E_t = \frac{e_t}{e_{ue}}$
$de_{d,i}$		The energy dissipated per displacement step	
$\Delta x_{ue,n}$	Velocity profile	The nodal traversal distance when pulse center moves one node forward	
v_i		The velocity of the center node in each displacement step	
m_b		Effective mass of a memory bit, used for kinetic energy calculation	
c_b	Damping coefficient	Memory bit damping coefficient	
e_{step}	Step energy	Nodal energy decrement when the pulse moves one node down the chain	
E_{min}		n.d. minimum value of e_{step} at which $v_i>0$ over the full range of the PEM	$E_{min} = \frac{e_{min}}{e_{ue}}$
E_{step}	n.d. step energy	n.d. decrement in nodal energy when the pulse moves one node down the chain	
e_d	dissipated energy	The dissipated energy of the moving pulse	
dt		The time increment while pulse moves from arrangement q to q+1.	
AND Gate			
l_{a1}, l_{a2}, l_{a3}		AND gate linkage lengths	$L_a = \frac{l_a}{x_{be}}$

k_{ad}	AND gate differential stiffness	Gate differential stiffness k_{ad} controls the energy released by the AND gate during the conjunct transition, boosting incoming pulse energy to raise the upper bound for the pulse to enter, but plays little role in the minimum stiffness at the output which lets the pulse leave.	$K_{ad} = \frac{k_{ad}}{k_{ac}}$
k_{acp3}	AND gate output port stiffness	Stiffness of the first coupling linkage after the output port	
k_{ac}	AND gate coupling stiffness	The stiffness of the coupling linkage located immediately before the AND gate output port.	
K_{ac}	AND gate impedance	AND gate coupling stiffness normalized with respect to k_{acp3}	$K_{ac} = \frac{k_{ac}}{k_{acp3}}$
x_{ap1}		x-direction displacement of AND gate input port 1 or 2, or output ap3	$X_{ap1} = \frac{x_{ap1}}{x_{be}}$
x_{ap3o}		x-direction displacement of AND gate output port uncompressed displacement	$X_{ap3o} = \frac{x_{ap3o}}{x_{be}}$
θ_{aa}, θ_{ab}		AND gate linkage angles	
$\theta_{aaMax}, \theta_{aaMax}$		AND gate linkage maximum allowable angles	
X_{ad}		n.d. differential displacement of AND gate inputs	$X_{ad} = \frac{x_{ad}}{x_{be}}$
X_{as}		n.d. shared displacement of AND gate inputs	$X_{as} = \frac{x_{as}}{x_{be}}$
X_{ac}		The compression n.d. displacement, derived by comparing the output motion, X_{ap3} to the uncompressed displacement, X_{ap3o}.	$X_{ac} = \frac{x_{ac}}{x_{be}}$
f_{ap1}		x-direction force of AND gate input port 1, 2 or 3	$F_{ap1} = \frac{f_{ap1}}{k_{ac} x_{be}}$
α_{aF}		Differential stiffness between the input ports of AND gate generates equal and opposite forces on the input gates, while compression stiffness generates a return force, captured by this term.	
k_{adMax}		Maximum possible AND gate differential stiffness	
e_{aDis}		Energy dissipated during the traversal of the pulse between nodes in the AND gate	
e_{aIn}		Minimum pulse energy valueat the AND gate inputs	
r_{kad}	Differential stiffness ratio	Captures the extent to which the pulse energy is routed to the AND gate differential mode	$r_{kpulse} = \frac{k_{bc}}{k_{bFmax}}$
r_{aE}	Energy ratio	Ratio of the AND gate output energy over the available energy after accounting for losses, and it determines the pulse energy at the gate output, which is generally set around 0.8 to ensure propagation despite fabrication variation	$r_{aE} = \frac{e_{aOut}}{e_{aOutMax}}$
$e_{aOutMax}$		Theoretical maximum energy output of the AND gate	

η_a	AND gate efficiency	Ratio of AND gate energy output over input. η_a will always be a lower than r_{aE}.	
x_{trans}		AND gate transition displacement of output node in x-direction. $x_{trans} \approx 0.98x_{be}$	
f_{bxp1}, f_{bxp2}		Nodal memory bit forces at the input 1 and 2 ports of AND gate	
$f_{ap1}, f_{ap2}, f_{ap3}$		Functions calculating the nodal AND gate forces at the input 1, 2 and output	
k_{cp1}, k_{cp2}		Coupling stiffnesses of the linkages to the input 1 and 2 ports of AND gate	
k_{bxp1}, k_{bxp2}		Memory bit bearing stiffnesses of AND gate input 1 and 2 ports	
$l_{a1trans}$		Modified l_{a1} to overcompensate the gate output ensures the incomplete input transitions still produce sufficient output displacement to drive pulse propagation	

Supplementary information references

1. Van EijK, J. On The Design of Plate-Spring Mechanisms. (TU Delft, 1985).

2. Howell, L. L. Compliant mechanisms. in *21st century kinematics* 189–216 (Springer, 2013).

3. Farsari, M. & Chichkov, B. N. Two-photon fabrication. *Nat. Photonics* **3**, 450–452 (2009).

4. Zhou, X., Hou, Y. & Lin, J. A review on the processing accuracy of two-photon polymerization. *AIP Adv.* **5**, 030701 (2015).